

Nonlinear Legendre Spectral Finite Elements for Wind Turbine Blade Dynamics

Qi Wang^{*1}, Michael A. Sprague^{†1}, Jason Jonkman^{‡1} and Nick Johnson^{§2}

¹National Renewable Energy Laboratory, Golden, CO 80401

²Colorado School of Mines, Golden, CO 80401

This paper presents a numerical implementation and examination of a new nonlinear beam finite-element (FE) model for highly flexible wind turbine blades made of composite materials. The underlying model is the geometrically exact beam theory (GEBT) and spatial discretization is achieved with Legendre spectral finite elements (LSFEs). The displacement-based GEBT is presented, which includes the coupling effects that exist in composite structures and geometric nonlinearity. LSFEs are high-order finite elements with nodes located at the Gauss-Legendre-Lobatto points. LSFEs can be an order of magnitude more efficient than low-order finite elements for a given accuracy level. The LSFE code is implemented in the module called BeamDyn in the new FAST Modularization Framework for dynamic simulation of highly flexible composite-material wind turbine blades. The framework allows for fully interactive simulations of turbine blades in operating conditions. Numerical examples showing verification and LSFE performance are provided in the numerical examples section. It concludes that the implemented code can be used as a efficient high-fidelity beam tool in FAST.

I. Introduction

Wind power is becoming one of the most important renewable-energy sources in the United States. In recent years, the size of wind turbines has been increasing to lower the cost, which, because of weight restrictions, also leads to highly flexible turbine blades. This huge electro-mechanical system poses a significant challenge for engineering design and analysis. Although possible with modern super computers, direct three-dimensional (3D) structural analysis is so computationally expensive that engineers are always seeking for efficient high-fidelity simplified models.

Beam models are widely used to represent and analyze engineering structures that have one of its dimensions much larger than the other two. Many engineering components can be idealized as beams: bridges in civil engineering, joists and lever arms in heavy-machine industries, and helicopter rotor blades. The blades, tower, and shaft in a wind turbine system can be considered as beams. In the weight-critical applications of beam structures, like high-aspect-ratio wings in aerospace and wind energy, composite materials are attractive due to their superior strength-to-weight and stiffness-to-weight ratios. However, analysis of composite-materials structures is more difficult than their isotropic counterparts due to elastic-coupling effects. The geometrically exact beam theory (GEBT) first proposed by Reissner¹, is a method that has proven powerful for analysis of highly flexible composite beams in the helicopter engineering community. During the past several decades, much effort has been invested in this area. Simo² and Simo and Vu-Quoc³ extended Reissner's work to deal with three-dimensional (3D) dynamic problems. Jelenić and Crisfield⁴ implemented this theory using the finite-element method where a new approach for interpolating the rotation field was proposed that preserves the geometric exactness. Betsch and Steinmann⁵ circumvented the interpolation of rotation by introducing a re-parameterization of the weak form corresponding to the equations of motion of GEBT. It is noted that Ibrahimbegović and his colleagues implemented this theory for static⁶ and dynamic⁷ analysis. In contrast to the displacement-based implementations, the geometric exact beam theory has also been formulated by mixed finite elements where both the primary and dual field are independently interpolated⁸. In the mixed formulation, all of the necessary ingredients, including Hamilton's principle and kinematic equations, are combined in a single variational formulation statement; Lagrange multipliers, motion variables, generalized strains, forces and moments, linear and angular momenta, and displacement and rotation variables are considered as independent quantities. Yu et al.^{9,10} presented the implementation of GEBT in a mixed formulation; various rotation parameters were investigated and the code was validated against analytical and numerical solutions. Readers are referred to Hodges¹¹, where comprehensive derivations and discussions on nonlinear composite-beam theories can be found.

^{*}Research Engineer, National Wind Technology Center, AIAA Member. Email: Qi.Wang2@nrel.gov

[†]Senior Research Scientist, Scientific Computing Center, AIAA Member. Email: Michael.A.Sprague@nrel.gov

[‡]Senior Engineer, National Wind Technology Center, AIAA Member. Email: Jason.Jonkman@nrel.gov.

[§]Graduate Research Assistant, Department of Mechanical Engineering.

Legendre spectral finite elements^{12,13} (LSFEs) are p -type finite elements whose shape functions are Lagrangian interpolants with node locations at the Gauss-Lobatto-Legendre (GLL) points. LSFEs combine the accuracy of global spectral methods with geometric flexibility of h -type FEs. The spectral FEs have seen successful use in the simulation of fluid dynamics^{12–14}, two-dimensional elastic wave propagation in solid media in geophysics¹⁵, elastodynamics¹⁶, and acoustic wave propagation¹⁷. However, it has seen limited application to dynamic analysis of beam^{18–21,32} and plate elements^{22–24}. **COMMENT: we need to add references on "quadrature elements"**

In this paper, we present a displacement-based implementation of geometrically exact beam theory using LSFEs. This work builds on a previous effort which showed the implementation of three-dimensional rotation parameters¹⁰ and a demonstration example of two-dimensional nonlinear spectral beam elements²⁵ for static deformation. The code implemented in this work is in accordance to FAST Modularization Framework²⁶, which allows simulation of a whole turbine under realistic operating conditions. **COMMENT: EXPAND ON FAST MODULARIZATION**

The paper is organized as follows. The theoretical foundation of the geometrically exact beam theory is introduced first. Then the GEBT discretization by LSFEs is discussed. Finally, verification examples are provided to show the accuracy and efficiency of the GEBT LSFEs for isotropic and composite beams.

II. Geometrically Exact Beam Theory

For completeness, this section reviews the geometrically exact beam theory and linearization process of the governing equations. The content of this section can be found in many other papers and textbooks. Figure 1 shows a beam in its initial undeformed and deformed states. A reference frame \mathbf{b}_i , for $i = \{1, 2, 3\}$, is introduced along the beam axis for the undeformed state; a frame \mathbf{B}_i is introduced along each point of the deformed beam axis. Curvilinear-coordinate x_1 defines the intrinsic parameterization of the reference line; similarly, s denotes the deformed reference line.

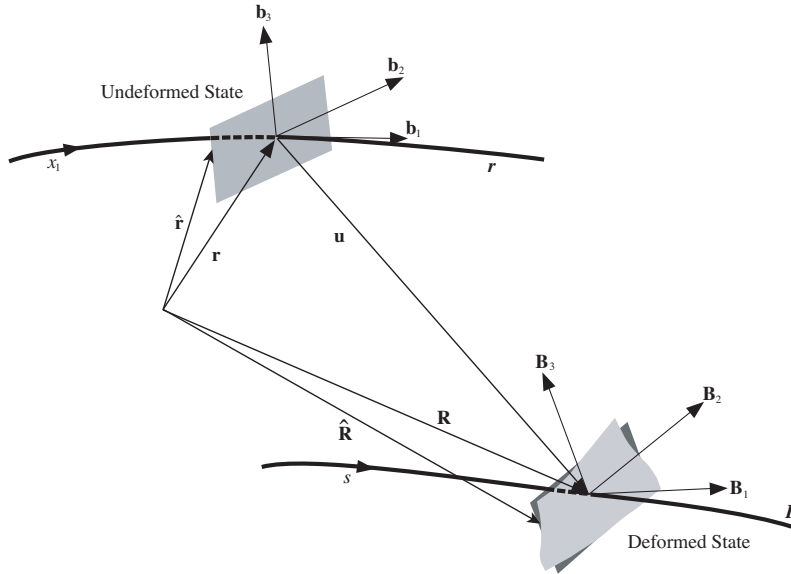


Figure 1: Schematic of a beam segment in its undeformed and deformed and its associated kinematic variables.

In this paper, we use matrix notation to denote vectorial or vectorial-like quantities. For example, we use a underline to denote a vector \underline{u} , a bar to denote unit vector \bar{n} , and double underline to denote a tensor $\underline{\underline{A}}$. Note that sometimes the underlines only denote the dimension of the corresponding matrix. The governing equations of motion for geometrically exact beam theory can be written as²⁷

$$\dot{\underline{h}} - \underline{F}' = \underline{f} \quad (1)$$

$$\dot{\underline{g}} + \tilde{\underline{u}}\underline{h} - \underline{M}' - (\tilde{x}_0' + \tilde{u}')\underline{F} = \underline{m} \quad (2)$$

where \underline{h} and \underline{g} are the linear and angular momenta resolved in the inertial coordinate system, respectively; \underline{F} and \underline{M} are the beam's sectional forces and moments, respectively; \underline{u} is the 1D displacement of the reference line; \underline{x}_0 is the initial position vector of a point along the beam's reference line; \underline{f} and \underline{m} are the distributed force and moment applied to the beam structure. A prime indicates a derivative with respect to the beam axis x_1 and an overdot indicates a derivative with respect to time. The tilde operator, i.e., $\tilde{(\cdot)}$, denotes a second-order, skew-symmetric tensor corresponding to the

given vector. In the literature, it is also termed as "cross-product matrix". For example, for the vector \bar{n} ,

$$\tilde{n} = \begin{bmatrix} 0 & -n_3 & n_2 \\ n_3 & 0 & -n_1 \\ -n_2 & n_1 & 0 \end{bmatrix}$$

The constitutive equations relate the velocities to the momenta and the one-dimensional strain measures to the sectional resultants as

$$\begin{Bmatrix} \underline{h} \\ \underline{g} \end{Bmatrix} = \underline{\underline{M}} \begin{Bmatrix} \underline{\dot{u}} \\ \underline{\dot{\omega}} \end{Bmatrix} \quad (3)$$

$$\begin{Bmatrix} \underline{F} \\ \underline{M} \end{Bmatrix} = \underline{\underline{C}} \begin{Bmatrix} \underline{\epsilon} \\ \underline{\kappa} \end{Bmatrix} \quad (4)$$

where $\underline{\underline{M}}$ and $\underline{\underline{C}}$ are the 6×6 sectional mass and stiffness matrices, respectively, note that they are not really tensors; $\underline{\epsilon}$ and $\underline{\kappa}$ are the 1D strains and curvatures, respectively. $\underline{\omega}$ is the angular velocity vector that is defined by the rotation tensor \underline{R} as $\underline{\omega} = \text{axial}(\underline{\dot{R}} \underline{R})$.

For a displacement-based finite element implementation, there are six degree-of-freedom (DoFs) at each node: 3 displacement components and 3 rotation components. Here we use \underline{q} to denote the elemental displacement array as $\underline{q} = [\underline{u}^T \ \underline{p}^T]^T$ where \underline{u} is the 1D displacement and \underline{p} is the rotation parameter vector. The acceleration array can thus be defined as $\underline{a} = [\underline{\ddot{u}}^T \ \underline{\dot{\omega}}^T]^T$. For nonlinear finite element analysis, the discretized and incremental forms of displacement, velocity, and acceleration array are written as

$$\underline{q}(x_1) = \underline{\underline{N}} \hat{\underline{q}} \quad \Delta \underline{q}^T = [\Delta \underline{u}^T \ \Delta \underline{p}^T] \quad (5)$$

$$\underline{v}(x_1) = \underline{\underline{N}} \hat{\underline{v}} \quad \Delta \underline{v}^T = [\Delta \underline{\dot{u}}^T \ \Delta \underline{\dot{\omega}}^T] \quad (6)$$

$$\underline{a}(x_1) = \underline{\underline{N}} \hat{\underline{a}} \quad \Delta \underline{a}^T = [\Delta \underline{\ddot{u}}^T \ \Delta \underline{\dot{\omega}}^T] \quad (7)$$

where $\underline{\underline{N}}$ is the shape function matrix and (\bullet) denotes a column matrix of nodal values. It is noted that given the "untensorial" nature, we need to adopt some special algorithm to deal with the 3D rotations which will be introduced in the next section. The governing equations for beams are highly nonlinear so that a linearization process is needed. According to Bauchau²⁷, the linearized governing equations in Eq. (1) and (2) are in the form of

$$\underline{\underline{\hat{M}}} \Delta \hat{\underline{a}} + \underline{\underline{\hat{G}}} \Delta \hat{\underline{v}} + \underline{\underline{\hat{K}}} \Delta \hat{\underline{q}} = \underline{\hat{F}}^{ext} - \underline{\hat{F}} \quad (8)$$

where the $\underline{\underline{\hat{M}}}$, $\underline{\underline{\hat{G}}}$, and $\underline{\underline{\hat{K}}}$ are the elemental mass, gyroscopic, and stiffness matrices, respectively; $\underline{\hat{F}}$ and $\underline{\hat{F}}^{ext}$ are the elemental forces and externally applied loads, respectively. They are defined as follows

$$\underline{\underline{\hat{M}}} = \int_0^l \underline{\underline{N}}^T \underline{\underline{M}} \underline{\underline{N}} dx_1 \quad (9)$$

$$\underline{\underline{\hat{G}}} = \int_0^l \underline{\underline{N}}^T \underline{\underline{G}}^I \underline{\underline{N}} dx_1 \quad (10)$$

$$\underline{\underline{\hat{K}}} = \int_0^l \left[\underline{\underline{N}}^T (\underline{\underline{K}}^I + \underline{\underline{Q}}) \underline{\underline{N}} + \underline{\underline{N}}^T \underline{\underline{P}} \underline{\underline{N}}' + \underline{\underline{N}}'^T \underline{\underline{C}} \underline{\underline{N}}' + \underline{\underline{N}}'^T \underline{\underline{Q}} \underline{\underline{N}} \right] dx_1 \quad (11)$$

$$\underline{\hat{F}} = \int_0^l (\underline{\underline{N}}^T \underline{\underline{F}}^I + \underline{\underline{N}}^T \underline{\underline{F}}^D + \underline{\underline{N}}'^T \underline{\underline{F}}^C) dx_1 \quad (12)$$

$$\underline{\hat{F}}^{ext} = \int_0^l \underline{\underline{N}}^T \underline{\underline{F}}^{ext} dx_1 \quad (13)$$

The new matrix notations in Eq. (9) to (13) are briefly introduced here. $\underline{\underline{M}}$ is the sectional mass matrix resolved in inertial system; $\underline{\underline{F}}^C$ and $\underline{\underline{F}}^D$ are elastic forces obtained from Eq. (1) and (2) as

$$\underline{\underline{F}}^C = \begin{Bmatrix} \underline{F} \\ \underline{M} \end{Bmatrix} = \underline{\underline{C}} \begin{Bmatrix} \underline{\epsilon} \\ \underline{\kappa} \end{Bmatrix} \quad (14)$$

$$\underline{\underline{F}}^D = \begin{bmatrix} \underline{0} & \underline{0} \\ (\underline{\hat{x}}'_0 + \underline{\hat{u}}')^T & \underline{0} \end{bmatrix} \underline{\underline{F}}^C \equiv \underline{\underline{\Upsilon}} \underline{\underline{F}}^C \quad (15)$$

where $\underline{\underline{0}}$ denotes a 3×3 null matrix. The $\underline{\underline{G}}^I$, $\underline{\underline{K}}^I$, $\underline{\underline{Q}}$, $\underline{\underline{P}}$, $\underline{\underline{Q}}$, and $\underline{\underline{F}}^I$ in Eq. (10), Eq. (11), and Eq. (12) are defined as

$$\underline{\underline{G}}^I = \begin{bmatrix} \underline{\underline{0}} & (\tilde{\omega} m \tilde{\eta})^T + \tilde{\omega} m \tilde{\eta}^T \\ \underline{\underline{0}} & \tilde{\omega} \underline{\underline{Q}} - \underline{\underline{Q}} \tilde{\omega} \end{bmatrix} \quad (16)$$

$$\underline{\underline{K}}^I = \begin{bmatrix} \underline{\underline{0}} & \dot{\tilde{\omega}} m \tilde{\eta}^T + \tilde{\omega} \tilde{\omega} m \tilde{\eta}^T \\ \underline{\underline{0}} & \ddot{u} m \tilde{\eta} + \underline{\underline{Q}} \dot{\tilde{\omega}} - \underline{\underline{Q}} \tilde{\omega} + \tilde{\omega} \underline{\underline{Q}} \tilde{\omega} - \tilde{\omega} \underline{\underline{Q}} \tilde{\omega} \end{bmatrix} \quad (17)$$

$$\underline{\underline{Q}} = \begin{bmatrix} \underline{\underline{0}} & \underline{\underline{C}}_{11} \tilde{E}_1 - \tilde{F} \\ \underline{\underline{0}} & \underline{\underline{C}}_{21} \tilde{E}_1 - \tilde{M} \end{bmatrix} \quad (18)$$

$$\underline{\underline{P}} = \begin{bmatrix} \underline{\underline{0}} & \underline{\underline{0}} \\ \tilde{F} + (\underline{\underline{C}}_{11} \tilde{E}_1)^T & (\underline{\underline{C}}_{21} \tilde{E}_1)^T \end{bmatrix} \quad (19)$$

$$\underline{\underline{Q}} = \underline{\underline{\Upsilon}} \underline{\underline{Q}} \quad (20)$$

$$\underline{\underline{F}}^I = \begin{Bmatrix} m \ddot{u} + (\dot{\tilde{\omega}} + \tilde{\omega} \tilde{\omega}) m \tilde{\eta} \\ m \tilde{\eta} \ddot{u} + \underline{\underline{Q}} \dot{\tilde{\omega}} + \tilde{\omega} \underline{\underline{Q}} \tilde{\omega} \end{Bmatrix} \quad (21)$$

where the following notations were introduced to simplify the writing of the above expressions

$$\underline{E}_1 = \underline{x}'_0 + \underline{u}' \quad (22)$$

$$\underline{\underline{C}} = \begin{bmatrix} \underline{\underline{C}}_{11} & \underline{\underline{C}}_{12} \\ \underline{\underline{C}}_{21} & \underline{\underline{C}}_{22} \end{bmatrix} \quad (23)$$

The derivation and linearization of governing equations of geometrically exact beam theory can be found in Bauchau²⁷.

It is pointed out that the three-dimensional rotations are represented by Wiener-Milenković parameters^{10,28} defined in the following equation:

$$\underline{p} = 4 \tan \left(\frac{\phi}{4} \right) \bar{n} \quad (24)$$

where ϕ is the rotation angle and \bar{n} is the unit vector of rotation axis. It can be observed that the valid range for this parameter is $|\phi| < 2\pi$ where a singularity point will be reached at 2π . The singularities existing at multiples of $\pm 2\pi$ in the above definition can be removed by a rescaling operation at π , as given in Ref²⁸:

$$\underline{r} = \begin{cases} 4(q_0 \underline{p} + p_0 \underline{q} + \tilde{p} \underline{q}) / (\Delta_1 + \Delta_2), & \text{if } \Delta_2 \geq 0 \\ -4(q_0 \underline{p} + p_0 \underline{q} + \tilde{p} \underline{q}) / (\Delta_1 - \Delta_2), & \text{if } \Delta_2 < 0 \end{cases} \quad (25)$$

where \underline{p} , \underline{q} , and \underline{r} are the vectorial parameterization of three finite rotations such that $\underline{R}(\underline{r}) = \underline{R}(\underline{p})\underline{R}(\underline{q})$; $p_0 = 2 - \underline{p}^T \underline{p} / 8$, $q_0 = 2 - \underline{q}^T \underline{q} / 8$, $\Delta_1 = (4 - p_0)(4 - q_0)$, and $\Delta_2 = p_0 q_0 - \underline{p}^T \underline{q}$. It is noted that the rescaling operation could cause discontinuity of the interpolated rotational field; therefore a more robust interpolation algorithm will be introduced in the next section where the rescaling-independent relative rotation field are interpolated.

III. Numerical Implementation by Legendre Spectral Finite Elements

The displacement fields in a element are approximated as

$$\underline{u}(\xi) = h^k(\xi) \hat{\underline{u}}^k \quad (26)$$

$$\underline{u}'(\xi) = h^{k'}(\xi) \hat{\underline{u}}^k \quad (27)$$

where $h^k(\xi)$ is the p^{th} -order polynomial Lagrangian-interpolant shape function of node k , $k = \{1, 2, \dots, p+1\}$, $\hat{\underline{u}}^k$ is the k^{th} nodal value, and $\xi \in [-1, 1]$ is the element natural coordinate. However, as discussed in Bauchau et al.²⁹, the three-dimensional rotation field cannot be simply interpolated as the displacement field in the form of

$$\underline{c}(\xi) = h^k(\xi) \hat{\underline{c}}^k \quad (28)$$

$$\underline{c}'(\xi) = h^{k'}(\xi) \hat{\underline{c}}^k \quad (29)$$

where \underline{c} is the rotation field in a element and $\hat{\underline{c}}^k$ is the nodal value at the k^{th} node, for three reasons: 1) rotations do not form a linear space so that they must be “composed” instead of added; 2) a rescaling operation is needed to eliminate the singularity existing in the vectorial rotation parameters; 3) the rotation field lacks objectivity, which, as defined by Crisfield and Jelenić⁴, refers to the invariance of strain measures computed through interpolation to the addition of a rigid-body motion. Therefore, we adopt the more robust interpolation approach proposed by Crisfield and Jelenić⁴ to deal with the finite rotations. Our approach is described as follows

Step 1: Compute the nodal relative rotations, $\hat{\underline{r}}^k$ by removing the reference rotation, $\hat{\underline{c}}^1$, from the finite rotation at each node, $\hat{\underline{r}}^k = \hat{\underline{c}}^{1-} \oplus \hat{\underline{c}}^k$.

Step 2: Interpolate the relative rotation field: $\underline{r}(\xi) = h^k(\xi)\hat{\underline{r}}^k$ and $\underline{r}'(\xi) = h^{k'}(\xi)\hat{\underline{r}}^k$. Find the curvature field $\underline{k}(\xi) = \underline{\underline{H}}(\hat{\underline{c}}^1)\underline{\underline{H}}(\underline{r})\underline{r}'$.

Step 3: Restore the rigid body rotation removed in Step 1: $\underline{c}(\xi) = \hat{\underline{c}}^1 \oplus \underline{r}(\xi)$.

where $\underline{\underline{H}}$ is the tangent tensor that relates the curvature vector \underline{k} and rotation vector \underline{p} as

$$\underline{k} = \underline{\underline{H}} \underline{p}' \quad (30)$$

Note that the relative rotation field can be computed with respect to any of the nodes of the element; and we choose node 1 as the reference node for convenient. In the LSFE approach, shape functions (e.g., those composing \underline{N}) are p^{th} -order Lagrangian interpolants, where nodes are located at the $p + 1$ GLL-quadrature points in the $[-1, 1]$ element natural-coordinate domain. Figure 2 shows representative LSFE basis functions for fourth- and eighth-order elements. Note that nodes are clustered near element endpoints. In the present implementation, weak-form integrals are evaluated with p -point reduced Gauss quadrature.

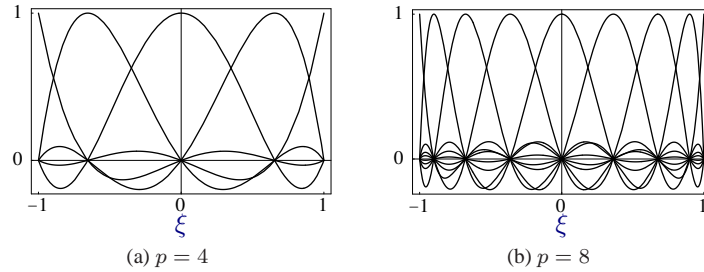


Figure 2: Representative $p + 1$ Lagrangian-interpolant shape functions in the element natural coordinates for (a) fourth- and (b) eighth-order LSFEs, where nodes are located at the Gauss-Lobatto-Legendre points.

The geometrically exact beam theory introduced above has been implemented using Legendre spectral finite element, known as BeamDyn, as a module functioning in the FAST modularization framework. The system of nonlinear equations in Eq. (1) and (2) are solved using Newton-Raphson method in the linearized form in Eq. (8) at each iteration for corrections to the nodal displacements and rotations until convergence is reached. In the present implementation, a energy-like stopping criterion has been chosen, which is calculated as

$$\|\Delta \mathbf{U}^{(i)T} \left({}^{t+\Delta t} \mathbf{R} - {}^{t+\Delta t} \mathbf{F}^{(i-1)} \right)\| \leq \|\epsilon_E \left(\Delta \mathbf{U}^{(1)T} \left({}^{t+\Delta t} \mathbf{R} - {}^t \mathbf{F} \right) \right)\| \quad (31)$$

where $\|\cdot\|$ denotes the Euclidean norm, $\Delta \mathbf{U}$ is the incremental displacement vector, \mathbf{R} is the vector of externally applied nodal point loads, \mathbf{F} is the vector of nodal point forces corresponding to the internal element stresses, and ϵ_E is the preset energy tolerance. The superscript on the left side of a variable denotes the time step number while the one on the right side denotes the Newton-Raphson iteration number. As pointed out by Bathe and Cimento³⁰, this criterion provides information of when both the displacements and the forces are near their equilibrium values. Time integration is performed using the generalized- α scheme in BeamDyn, which is an unconditionally stable, second-order accurate algorithm. The users can choose proper parameters to achieve high frequency numerical dissipation in this scheme. More details regarding the generalized- α method can be found in Refs.^{27,31}.

IV. Numerical Examples

A. Example 1: Static bending of a cantilever beam

The first example is a common benchmark problem for geometrically nonlinear analysis of beams^{2,32}. We calculate the static deflection of a cantilever beam that is subjected at its free end to a constant moment about the x_2 axis, M_2 ; a system schematic is shown in Figure 3. The length of the beam L is 10 inches and the cross-sectional stiffness matrix is

$$\mathbf{C}^* = 10^3 \times \begin{bmatrix} 1770 & 0 & 0 & 0 & 0 & 0 \\ 0 & 1770 & 0 & 0 & 0 & 0 \\ 0 & 0 & 1770 & 0 & 0 & 0 \\ 0 & 0 & 0 & 8.16 & 0 & 0 \\ 0 & 0 & 0 & 0 & 86.9 & 0 \\ 0 & 0 & 0 & 0 & 0 & 215 \end{bmatrix} \quad (32)$$

Table 1: Comparison of analytical and BeamDyn-calculated tip axial displacement u_1 of a cantilever beam subject to a constant moment (in inches); the BeamDyn model was composed of two 5^{th} -order LSFES.

λ	Analytical	BeamDyn
0.4	-2.4317	-2.4317
0.8	-7.6613	-7.6613
1.2	-11.5591	-11.5591
1.6	-11.8921	-11.8921
2.0	-10.0000	-10.0000

which has units of C_{ij}^* (lb), $C_{i,j+3}^*$ (lb.in), and $C_{i+3,j+3}^*$ (lb.in²) for $i, j = 1, 2, 3$; these units apply to all subsequent stiffness matrices. It is pointed out that the term with an asterisk denotes that it is resolved in the material coordinate system.

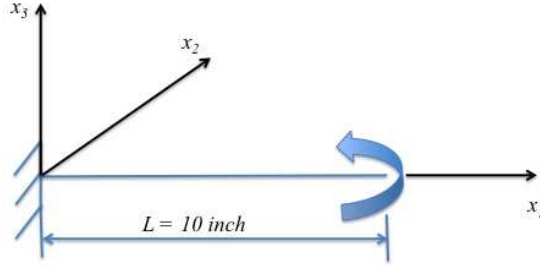


Figure 3: Schematic of a cantilever beam with tip moment, which was used in BeamDyn verification and performance studies.

The load applied at the tip is given by

$$M_2 = \lambda \bar{M}_2 \quad (33)$$

where $\bar{M}_2 = \pi \frac{EI_2}{L}$; and the parameter λ will vary between 0 and 2. In this case, the beam is discretized with two 5^{th} -order Legendre spectral FEs. The static deformations of the beam obtained from BeamDyn are shown in Figure 4 for six different tip moments. The calculated tip displacements are compared with the analytical solution, which can be found in Mayo et al.³³ as

$$u_1 = \rho \sin\left(\frac{x_1}{\rho}\right) - x_1 \quad u_3 = \rho \left(1 - \cos\left(\frac{x_1}{\rho}\right)\right) \quad (34)$$

Analytical and BeamDyn-calculated results can be found in Table 1 and 2. At this discretization level, BeamDyn results are virtually identical to those of the analytical solution.

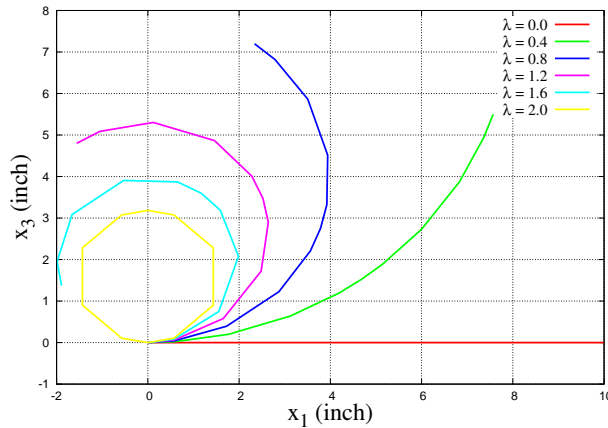


Figure 4: Static deflection of a cantilever beam under six constant bending moments as calculated with two 5^{th} -order Legendre spectral FEs in BeamDyn.

The rotation parameter p_2 at each node along beam axis x_1 obtained from BeamDyn are plotted in Figure 5a for $\lambda = 0.8$ and $\lambda = 2.0$, respectively. A rescaling can be observed from this figure for the case $\lambda = 2.0$. It is

Table 2: Comparison of analytical and BeamDyn-calculated tip vertical displacement u_3 of a cantilever beam subject to a constant moment (in inches); the BeamDyn model was composed of two 5^{th} -order LSFES.

λ	Analytical	BeamDyn
0.4	5.4987	5.4987
0.8	7.1978	7.1979
1.2	4.7986	4.7986
1.6	1.3747	1.3747
2.0	0.0000	0.0000

noted that although the rotation parameters are not continuous between elements due to the rescaling operation, the relatively rotations are continuous in a single element as described in the previous section, which can be observed from Figure 5b.

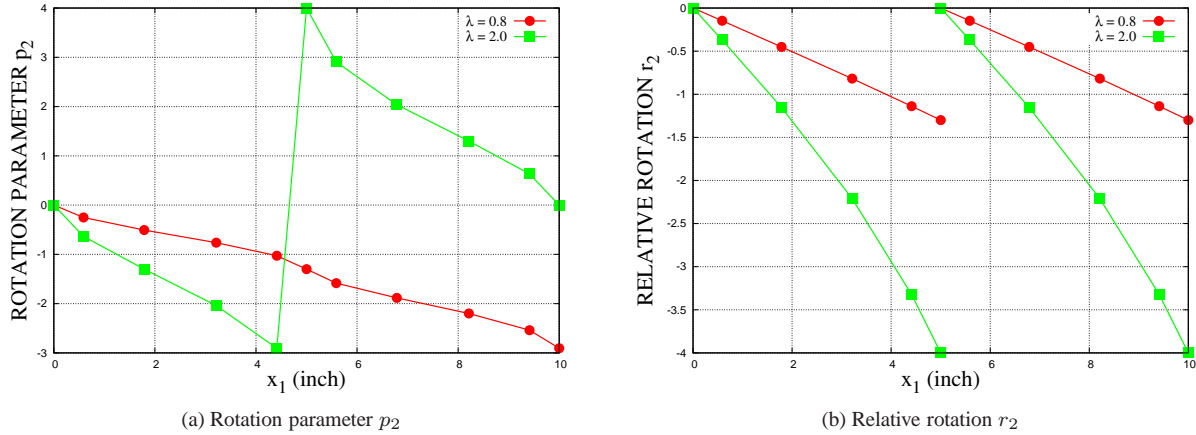


Figure 5: (a) Wiener-Milenković rotation parameters along beam axis x_1 as calculated by BeamDyn for two tip moments; (b) Relative rotations in two elements for the cases of $\lambda = 0.8$ and $\lambda = 2.0$.

Finally, we conduct a convergence study of the BeamDyn LSFES. The convergence rate is compared with conventional quadratic elements used in Dymore³⁴, which is a finite-element based multibody dynamics code for the comprehensive modeling of flexible multibody systems. Figure 6 shows the normalized error $\varepsilon(u)$, where u is the calculated tip displacement (at $x = L$), as a function of the number of model nodes for the calculation with Dymore quadratic finite elements (QFE) and a single Legendre spectral element finite (LSFE), where

$$\varepsilon(u) = \left| \frac{u - u^a}{u^a} \right| \quad (35)$$

and where u^a is the analytical solution. The parameter λ is set to 1.0 for this case. The Legendre spectral elements (with p -refinement) exhibit highly desirable exponential convergence to machine-precision error, whereas the conventional quadratic elements are limited to algebraic convergence. For a given model size, an LSFE model can be orders of magnitude more accurate than its QFE counterpart.

B. Example 2: Static analysis of a composite beam

The second example is to show the capability of BeamDyn for composite beams with elastic couplings. The cantilever beam used in this case is 10 inches long with a boxed cross-section made of composite materials that can be found in Yu et al.³⁵. Readers are referred to Figure 3 for a schematic of this example system. The stiffness matrix is given as

$$C^* = 10^3 \times \begin{bmatrix} 1368.17 & 0 & 0 & 0 & 0 & 0 \\ 0 & 88.56 & 0 & 0 & 0 & 0 \\ 0 & 0 & 38.78 & 0 & 0 & 0 \\ 0 & 0 & 0 & 16.96 & 17.61 & -0.351 \\ 0 & 0 & 0 & 17.61 & 59.12 & -0.370 \\ 0 & 0 & 0 & -0.351 & -0.370 & 141.47 \end{bmatrix} \quad (36)$$

A concentrated force $P = 150 \text{ lbs}$ along the x_3 direction is applied at the free tip. In the BeamDyn analysis, the beam is meshed with two 5^{th} -order elements. The displacements and rotation parameters at each node along beam axis are

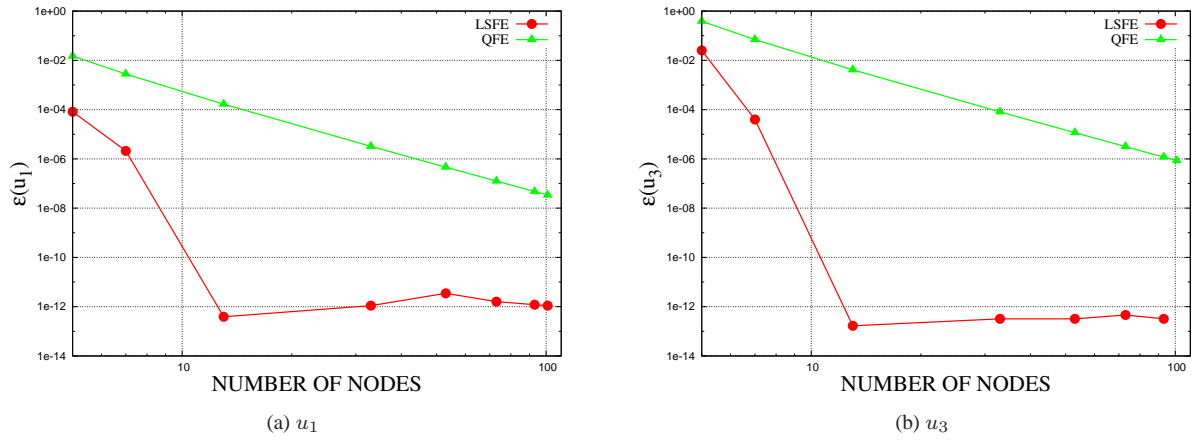


Figure 6: Normalized error of the (a) u_1 and (b) u_3 tip displacements of a cantiler beam (Figure 3) under constant tip moment ($\lambda = 1.0$) as a function of the total number of nodes. Results were calculated with BeamDyn (LSFE) and Dymore (QFE). LSFE model refinement was accomplished by increasing polynomial order and QFE model refinement was accomplished by increasing the number of elements.

Table 3: Numerically determined tip displacements and rotation parameters of a composite beam in Example 2 as calculated by BeamDyn (LSFE) and Dymore (QFE)

	u_1 (inch)	u_2 (inch)	u_3 (inch)	p_1	p_2	p_3
BeamDyn	-0.09064	-0.06484	1.22998	0.18445	-0.17985	0.00488
Dymore	-0.09064	-0.06483	1.22999	0.18443	-0.17985	0.00488

plotted in Figure 7. It is noted that the coupling effects exist between twist and two bendings. The applied in-plane force leads to a fairly large twist angle due to the bending-twist coupling, which can be observed in Figure 7b.

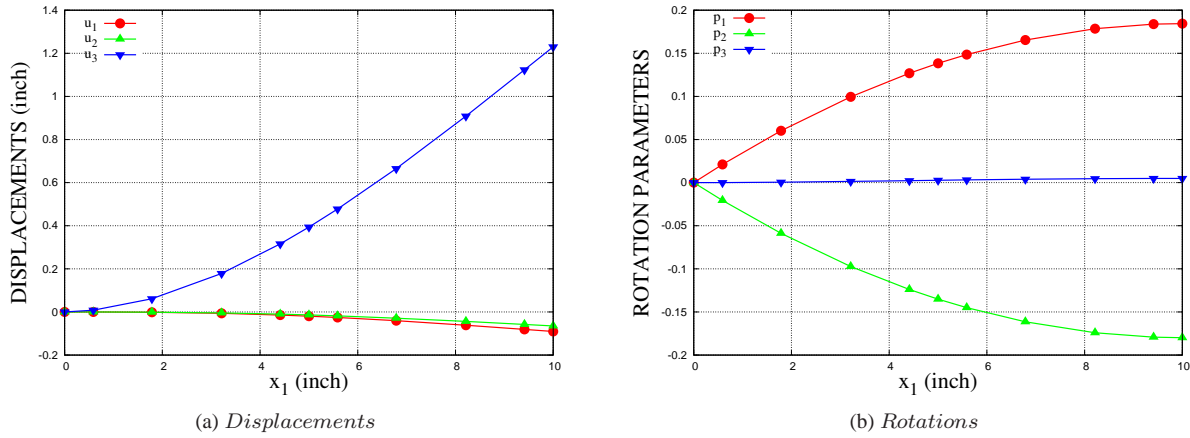


Figure 7: Displacements and rotation parameters along beam axis for Example 2.

The tip displacements and rotations are compared with those obtained by Dymore in Table 3 for verification, where the beam is meshed with 10 3rd-order elements. Good agreement can be observed between BeamDyn and Dymore results.

C. Example 3: dynamic analysis of a composite beam under sinusoidal force at the tip

The last example is a transient analysis of a composite beam with boxed cross-section that is used in Example 2. The beam has the same geometry and boundary conditions as the one in previous example. The mass sectional properties

are given by VABS^{35,36} as

$$M^* = 10^{-2} \times \begin{bmatrix} 8.538 & 0 & 0 & 0 & 0 & 0 \\ 0 & 8.538 & 0 & 0 & 0 & 0 \\ 0 & 0 & 8.538 & 0 & 0 & 0 \\ 0 & 0 & 0 & 1.4433 & 0 & 0 \\ 0 & 0 & 0 & 0 & 0.40972 & 0 \\ 0 & 0 & 0 & 0 & 0 & 1.0336 \end{bmatrix} \quad (37)$$

The units associated with the mass matrix values are M_{ii}^* (lb.s²/in²) and $M_{i+3,i+3}^*$ (lb.s²) for $i = 1, 2, 3$. The beam is divided into two 5th-order elements in the current calculation and a sinusoidal point force is applied at the free tip in the x_3 direction given as

$$P = A_F \sin(\omega_F t) \quad (38)$$

where $A_F = 1.0 \times 10^2$ lbs and $\omega_F = 10$ rad/s (see Figure 8). The time step used in this example is 0.005s so that a set of converged results can be achieved. The tip displacement and rotation histories of the beam are plotted in Figure 9. Note that all the components, including three displacements and three rotations, are non-zero due to the elastic coupling effects. The time histories of the stress resultants at the root of the beam are given in Figure 10.

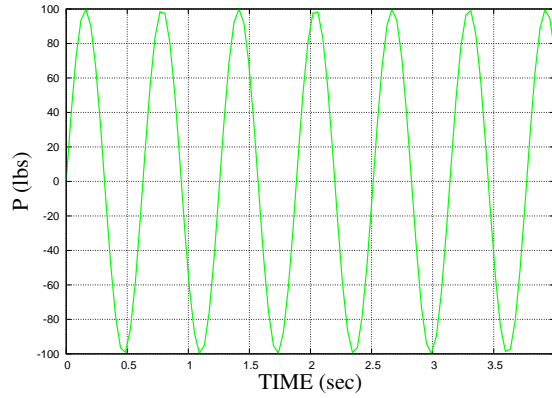


Figure 8: The applied sinusoidal vertical force at the tip in Example 3 .

Finally, we examine here the convergence rates of the LSFs and conventional quadratic elements (in Dymore). Figure 11 shows normalized root-mean-square (RMS) error of the numerical solutions for the displacement u_1 at the free tip over the time interval $0 \leq t \leq 4$. Normalized RMS error for n_{max} numerical response values u_1^n , where $u_1^n \approx u_1(t^n)$, was calculated as

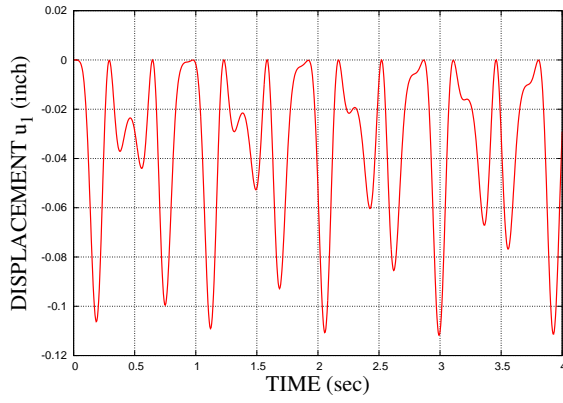
$$\varepsilon_{\text{RMS}}(u_1) = \sqrt{\frac{\sum_{k=0}^{n_{max}} [u_1^k - u_b(t^k)]^2}{\sum_{k=0}^{n_{max}} [u_b(t^k)]^2}} \quad (39)$$

where $u_b(t)$ is the benchmark solution; here $u_b(t)$ is a highly resolved numerical solution obtained by BeamDyn with one 20th-order element and the time step is $\Delta t_b = 1.0 \times 10^{-4}$. Two time-increment sizes are examined in the test calculations: $\Delta t_1 = 5.0 \times 10^{-3}$ and $\Delta t_2 = \frac{\Delta t_1}{2}$. The following observations can be made from Figure 11:

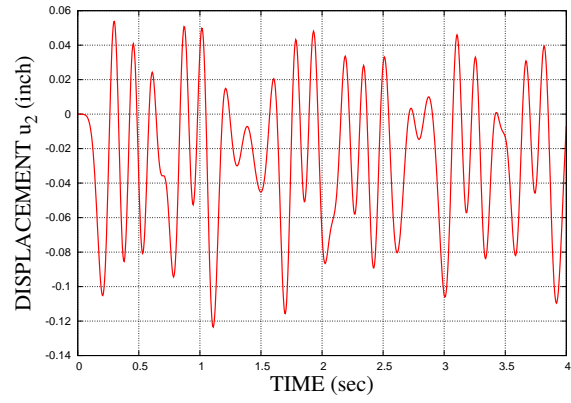
- For a fixed Δt , both Dymore (QFEs) and BeamDyn (LSFs) converge with spatial refinement to the same error level. BeamDyn is converged with only five nodes, whereas Dymore requires at least 9 nodes.
- The converged error levels are due exclusively to time-discretization error. We note that the converged error for $\Delta t_2 = \Delta t_1/2$ is one-fourth that for Δt_1 , which is expected for our second-order-accurate time integrator.

V. Conclusion

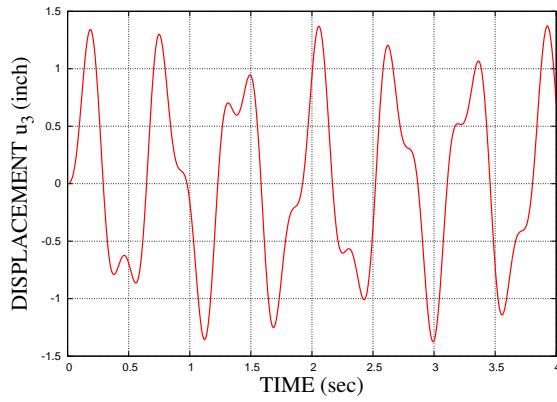
This paper presents a displacement-based implementation of geometrically exact beam theory. The Legendre spectral finite elements are adopted to discretize the beam in the space domain. Numerical examples were presented that demonstrate the capability of BeamDyn, a beam solver for wind turbine analysis developed by NREL. A benchmark static problem for nonlinear beam was studied first. The agreement between the results calculated by BeamDyn and analytical solution are excellent. Moreover, a convergence study has been conducted where the convergence rate of Legendre spectral elements are compared with the conventional 2nd order elements. Exponential convergence rates



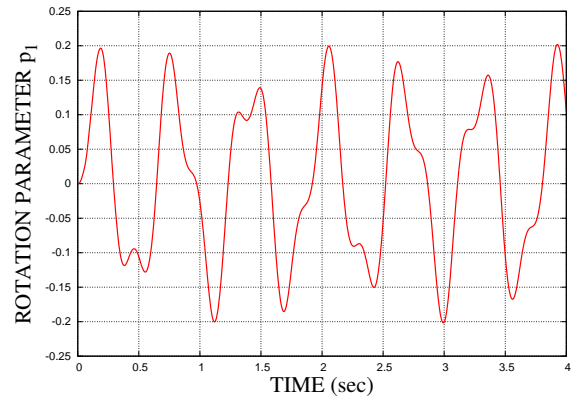
(a) u_1



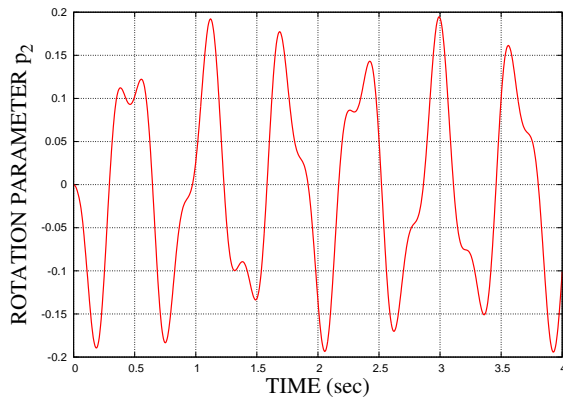
(b) u_2



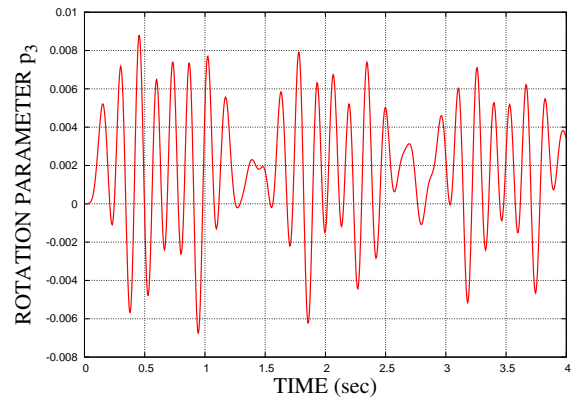
(c) u_3



(d) p_1

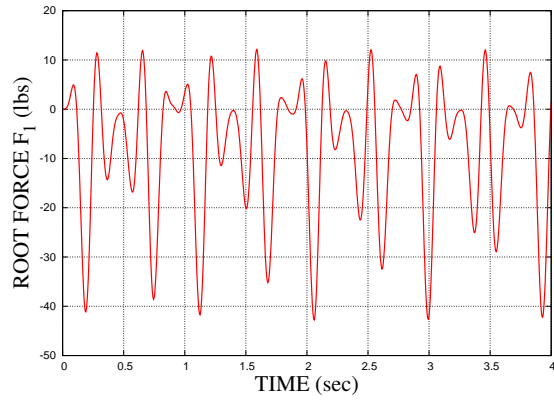


(e) p_2

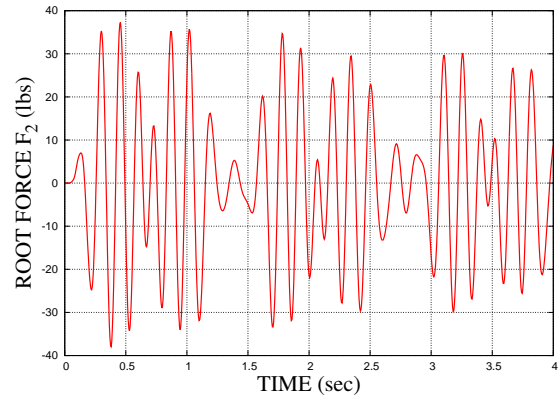


(f) p_3

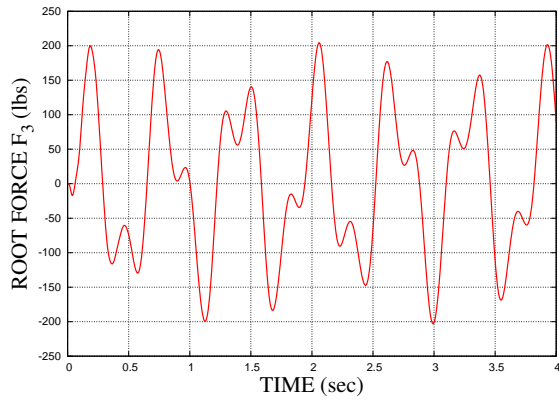
Figure 9: Tip displacement and rotation histories of a composite beam under vertical load.



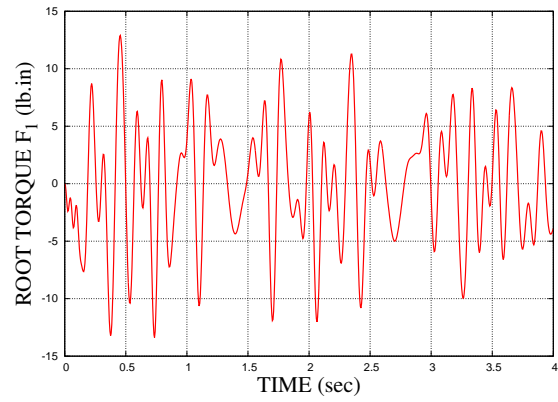
(a) F_1



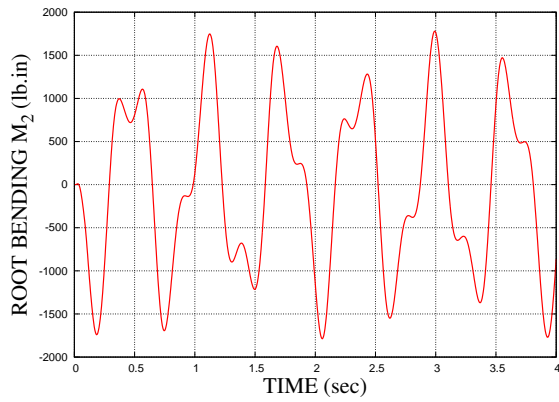
(b) F_2



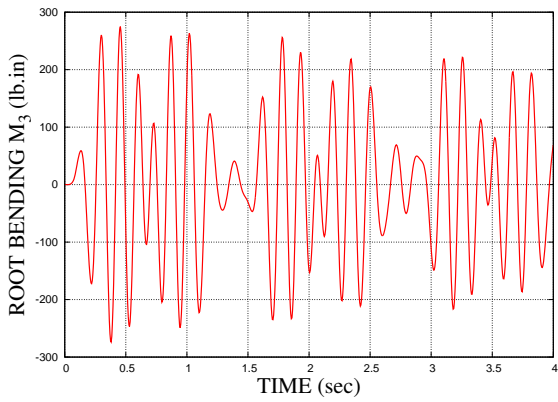
(c) F_3



(d) M_1



(e) M_2



(f) M_3

Figure 10: Stress resultant time histories at the root of a composite beam.

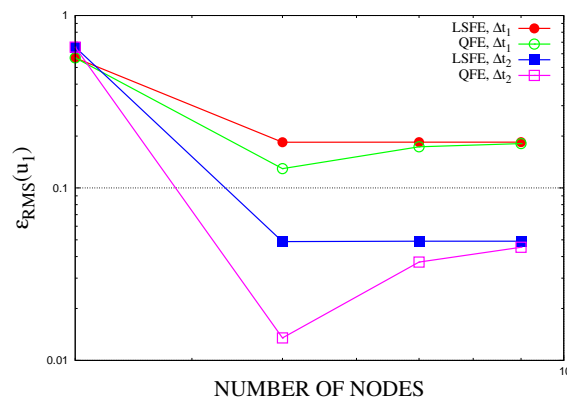


Figure 11: Normalized RMS error of tip displacement u_1 histories over $0 \leq t \leq 4$ as a function of number of nodes as cacluated by BeamDyn (LSFEs) and Dymore (QFEs).

were observed as expected for this type of element. A composite cantilever beam were studied both statically and dynamically. The static results are verified against those obtained by Dymore. The elastic coupling effects were shown in these two cases. It concludes that BeamDyn is a powerful tool for composite beam analysis that can be used as a module in the FAST modularization framework.

Acknowledgments

This work was supported by the U.S. Department of Energy under Contract No. DE-AC36-08-GO28308 with the National Renewable Energy Laboratory. Support was provided through a Laboratory Directed Research and Development grant *High-Fidelity Computational Modeling of Wind-Turbine Structural Dynamics*. The authors acknowledge Professor Oliver A. Bauchau for the technical discussions on the 3D rotation parameters.

References

- ¹Reissner, E., "On one-dimensional large-displacement finite-strain beam theory," *Studies in Applied Mathematics LII*, 1973, pp. 87–95.
- ²Simo, J. C., "A finite strain beam formulation. The three-dimensional dynamic problem. Part I," *Computer Methods in Applied Mechanics and Engineering*, Vol. 49, 1985, pp. 55–70.
- ³Simo, J. C. and Vu-Quoc, L., "A three-dimensional finite-strain rod model. Part II," *Computer Methods in Applied Mechanics and Engineering*, Vol. 58, 1986, pp. 79–116.
- ⁴Jelenić, G. and Crisfield, M. A., "Geometrically exact 3D beam theory: implementation of a strain-invariant finite element for statics and dynamics," *Computer Methods in Applied Mechanics and Engineering*, Vol. 171, 1999, pp. 141–171.
- ⁵Betsch, P. and Steinmann, P., "Frame-indifferent beam finite elements based upon the geometrically exact beam theory," *International Journal for Numerical Methods in Engineering*, Vol. 54, 2002, pp. 1775–1788.
- ⁶Ibrahimbegović, A., "On finite element implementation of geometrically nonlinear Reissner's beam theory: three-dimensional curved beam elements," *Computer Methods in Applied Mechanics and Engineering*, Vol. 122, 1995, pp. 11–26.
- ⁷Ibrahimbegović, A. and Mikdad, M. A., "Finite rotations in dynamics of beams and implicit time-stepping schemes," *International Journal for Numerical Methods in Engineering*, Vol. 41, 1998, pp. 781–814.
- ⁸Cook, R. D., Malkus, D. S., Plesha, M. E., and Witt, R. J., *Concepts and Applications of Finite Element Analysis*, Wiley, 4th ed., 2001.
- ⁹Yu, W. and Blair, M., "GEBT: A general-purpose nonlinear analysis tool for composite beams," *Composite Structures*, Vol. 94, 2012, pp. 2677–2689.
- ¹⁰Wang, Q., Yu, W., and Sprague, M. A., "Geometric nonlinear analysis of composite beams using Wiener-Milenković parameters," *Proceedings of the 54th Structures, Structural Dynamics, and Materials Conference*, Boston, Massachusetts, April 2013.
- ¹¹Hodges, D. H., *Nonlinear Composite Beam Theory*, AIAA, 2006.
- ¹²Patera, A. T., "A spectral element method for fluid dynamics: Laminar flow in a channel expansion," *Journal of Computational Physics*, Vol. 54, 1984, pp. 468–488.
- ¹³Ronquist, E. M. and Patera, A. T., "A Legendre spectral element method for the Stefan problem," *International Journal for Numerical Methods in Engineering*, Vol. 24, 1987, pp. 2273–2299.
- ¹⁴Deville, M. O., Fischer, P. F., and Mund, E. H., *High-order Methods for Incompressible Fluid Flow*, Cambridge University Press, 2002.
- ¹⁵Komatitsch, D. and Vilotte, J. P., "The spectral element method: and efficient tool to simulate the seismic response of 2D and 3D geological structures," *Bulletin of the Seismological Society of America*, Vol. 88, 1998, pp. 368–392.
- ¹⁶Sridhar, R., Chakraborty, A., and Gopalakrishnan, S., "Wave propagation in anisotropic and inhomogeneous untracked and cracked structures using the pseudo spectral finite element method," *International Journal of Solids and Structures*, Vol. 43, 2006, pp. 4997–5031.
- ¹⁷Sprague, M. A. and Geers, T. L., "A spectral-element method for modeling cavitation in transient fluid-structure interaction," *International Journal for Numerical Methods in Engineering*, Vol. 60, 2004, pp. 2467–2499.
- ¹⁸Ben-Tal, A., Bar-Yoseph, P. Z., and Flashner, H., "Optimal maneuver of a flexible arm by space-time finite element method," *Journal of Guidance, Control, and Dynamics*, Vol. 18, 1995, pp. 1459–1462.

- ¹⁹Ben-Tal, A., Bar-Yoseph, P. Z., and Flashner, H., "Space-time spectral element method for optimal slewing of a flexible beam," *International Journal for Numerical Methods in Engineering*, Vol. 39, 1996, pp. 3101–3121.
- ²⁰Kudela, P., Krawczuk, M., and Ostachowicz, W., "Wave propagation modeling in 1D structures using spectral finite elements," *Journal of Sound and Vibration*, Vol. 300, 2007, pp. 88–100.
- ²¹Sprague, M. A. and Geers, T. L., "Legendre spectral finite elements for structural dynamics analysis," *Communications in Numerical Methods in Engineering*, Vol. 24, 2008, pp. 1953–1965.
- ²²Zrahia, U. and Bar-Yoseph, P., "Plate spectral elements based upon Reissner-Mindlin theory," *International Journal for Numerical Methods in Engineering*, Vol. 38, 1995, pp. 1341–1360.
- ²³Kudela, P., Zak, A., Krawczuk, M., and Ostachowicz, W., "Modeling of wave propagation in composite plates using the time domain spectral element method," *Journal of Sound and Vibration*, Vol. 302, 2007, pp. 728–745.
- ²⁴Brito, K. D. and Sprague, M. A., "Reissner-Mindlin Legendre spectral finite elements with mixed reduced quadrature," *Finite Elements in Analysis and Design*, Vol. 58, 2012, pp. 74–83.
- ²⁵Wang, Q. and Sprague, M. A., "A Legendre spectral finite element implementation of geometrically exact beam theory," *Proceedings of the 54th Structures, Structural Dynamics, and Materials Conference*, Boston, Massachusetts, April 2013.
- ²⁶Jonkman, J. M., "The new modularization framework for the FAST wind turbine CAE tool," *Proceedings of the 51st AIAA Aerospace Sciences Meeting including the New Horizons Forum and Aerospace Exposition*, Grapevine, Texas, January 2013.
- ²⁷Bauchau, O. A., *Flexible Multibody Dynamics*, Springer, 2010.
- ²⁸Bauchau, O., Epple, A., and Heo, S., "Interpolation of finite rotations in flexible multibody dynamics simulations," *Proceedings of the Institution of Mechanical Engineers, Part K: Journal of Multi-body Dynamics*, Vol. 222, 2008, pp. 353–366.
- ²⁹Bauchau, O. A., Epple, A., and Bottasso, L., "Scaling of Constraints and Augmented Lagrangian Formulations in Multibody Dynamics Simulations," *Journal of Computational and Nonlinear Dynamics*, Vol. 4, 2009, pp. 021007–1–9.
- ³⁰Bathe, K. J. and Cimento, A. P., "Some practical procedures for the solution of nonlinear finite element equations," *Computer Methods in Applied Mechanics and Engineering*, Vol. 22, 1980, pp. 59–85.
- ³¹Chung, J. and Hulbert, G. M., "A time integration algorithm for structural dynamics with improved numerical dissipation: the generalized- α method," *Journal of Applied Mechanics*, Vol. 60, 1993, pp. 371–375.
- ³²Xiao, N. and Zhong, H., "Non-linear quadrature element analysis of planar frames based on geometrically exact beam theory," *International Journal of Non-Linear Mechanics*, Vol. 47, 2012, pp. 481–488.
- ³³Mayo, J. M., García-Vallejo, D., and Domínguez, J., "Study of the geometric stiffening effect: comparison of different formulations," *Multibody System Dynamics*, Vol. 11, 2004, pp. 321–341.
- ³⁴Bauchau, O. A., *Dymore User's Manual*.
- ³⁵Yu, W., Hodges, D. H., Volovoi, V., and Cesnik, C. E. S., "On Timoshenko-Like modeling of initially curved and twisted composite beams," *International Journal of Solids and Structures*, Vol. 39, 2002, pp. 5101–5121.
- ³⁶Wang, Q. and Yu, W., "Asymptotic multi physics modeling of composite slender structures," *Smart Materials and Structures*, Vol. 21, 2012, pp. 035002.